NUMERICAL INVESTIGATION ON THE AERODYNAMIC EFFECT OF MINI-TEDS ON THE AWIATOR AIRCRAFT AT CRUISE CONDITIONS

K. Richter*, H. Rosemann*
***German Aerospace Center (DLR), Bunsenstr. 10, 37073 Göttingen, Germany**

Keywords: *AWIATOR, mini-TED effect, split-flap, Reynolds-number influence, DLR-TAU code*

Abstract

Within the EU research project AWIATOR a numerical investigation on the aerodynamic effect of mini-TEDs on an Airbus A340-300 was conducted at wind-tunnel and free-flight conditions for cruise-flight Mach number and lift coefficients. An aircraft in cruise configuration with and without mini-TEDs applied to the wing trailing-edge was simulated with the DLR-TAU code. The mini-TEDs were realized by the use of split-flaps.

The numerical results show that lift is increased when using mini-TEDs and the wing-load distribution is changed with a re-distribution of lift towards the wing root as expected. The results achieve a good agreement with wind-tunnel experiments in terms of lift and drag as well as wing-surface pressure-distributions.

At free-flight conditions the mini-TED influence increases compared to wind-tunnel conditions. The lift-enhancing effect of mini-TEDs increases but the drag differences are affected unfavourably for the given aircraft configuration. The minimum lift coefficient of profitable mini-TED use is shifted to higher lift and the remaining drag reductions at high lift coefficients diminish.

Additional comparisons of numerical and flight-test pressure distributions for the baseline configuration show a good overall agreement.

Nomenclature

α	Angle of attack
η	Normalized spanwise position
c	Local wing chord
c_{AMC}	Aerodynamic mean chord
c_D	Drag coefficient
c_L	Lift coefficient
c_l	Local lift coefficient
c_p	Pressure coefficient
δ_{SF}	Split-flap deflection angle
l_{SF}	Split-flap length
M	Mach number
M_{max}	Maximal Mach number
mini-TED	Mini trailing-edge device
RANS	Reynolds averaged Navier-Stokes equations
Re	Reynolds number
x/c	Normalized x-coordinate
y^+	Normalized wall distance

1 Introduction

The European research project ‘Aircraft Wing with Advanced Technology Operation’ (AWIATOR) aims for the integration of new aerodynamic technologies into a modern transport aircraft. In task T3.3 ‘Adaptive Elements’ the use of adaptable mini trailing-edge devices (mini-TEDs) as part of a multifunctional control-surface system has been investigated [1], [2]. This has included the aerodynamic and structural design of adaptable mini-TEDs as well as their integration into the existing A340-300 aircraft. The aerodynamic design initiated by Airbus Germany has been carried out by numerical simulations and wind-tunnel tests for both take-off/landing and cruise conditions. The final aerodynamic assessment of the mini-TED system developed will be done in flight tests.

Various types of mini-TEDs were studied by other authors outside AWIATOR in the past, mainly in a more fundamental manner and focussing on a low-speed application at low Reynolds-number conditions. Gurney flaps, split-flaps or divergent trailing-edges were investigated on single- or multi-element airfoils and wings, e.g. [3], [4], [5]. However, hardly any investigations were conducted at cruise conditions [6], [7], especially at free-flight Reynolds numbers.

The present paper introduces the numerical investigation performed within AWIATOR. The aim of this investigation is to determine the aerodynamic effect of mini-TEDs on the complex aircraft aerodynamics at cruise conditions and to evaluate the Reynolds-number influence on the mini-TED effect. The project includes a validation of the predictive tools with wind-tunnel experiments and flight tests.

2 Numerical Tools

The numerical investigation was performed with the DLR-TAU code. The DLR-TAU code is a CFD software package for solving the Reynolds-averaged Navier-Stokes equations (RANS) [8], [9]. The DLR-TAU code uses hybrid grids and is based on a three-dimensional finite volume scheme integrating the RANS equations. Inviscid fluxes are calculated either by a Roe- or AUSM-type 2nd-order upwind scheme, or by employing a central method with scalar dissipation. Viscous fluxes are discretised using central differences. The gradients of the flow variables are determined by a Green-Gauß formula. The discretisation of the temporal gradients uses an explicit multi-step Runge-Kutta scheme. In order to accelerate the convergence to steady state, residual smoothing and a multigrid technique are implemented. The turbulence models available are different types of the one-equation Spalart-Allmaras model [10] as well as different two-equation kω- and kε-models. In addition to the flow solver a grid adaptation module is part of the TAU software package enabling the adaptation of the grid depending on the flow solution. Both the adaptation of height and distribution of the prismatic layers ('y^+'-adaptation) and the refinement of the flow field at locations of high gradients are provided.

The hybrid grids used for the RANS computations were generated using the commercial grid generation system CENTAUR™ [11]. CENTAUR™ provides a CAD converter for CAD cleaning and diagnostics and a hybrid-grid generator for surface, prismatic and tetrahedral grid generation.

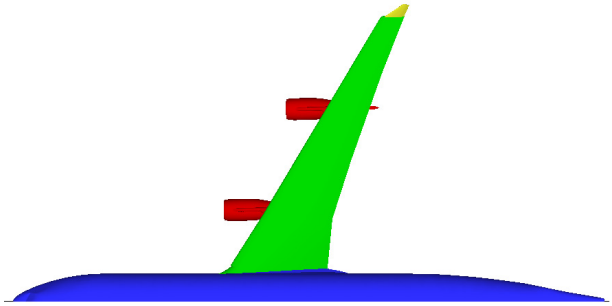

Fig. 1: AWIATOR aircraft in baseline configuration

3 Aircraft Configurations

The numerical investigation was conducted with the 'AWIATOR aircraft' based on an Airbus A340-300. Two cruise-flight configurations of the AWIATOR aircraft were investigated in flight shape: the baseline configuration with the standard clean wing and the mini-TED configuration with mini-TEDs applied to the wing trailing-edge. Both aircraft configurations were considered without tail-planes or flap-track fairings. Fig. 1 shows a top view of the AWIATOR aircraft in baseline configuration. It is a wing/body configuration with two engine nacelles including pylons and a winglet.

The mini-TEDs were realised by split-flaps that were integrated into the trailing edge of the wing. The deflection angle was given with $\delta_{SF} = 7.5°$ corresponding to wind-tunnel tests. Fig. 2 shows the trailing-edge geometry with retracted and deflected split-flap. The wing trailing-edge region was modelled in detail for both configurations, i.e. the gap existing between the deflected split-flap and the fixed part of the trailing-edge was taken into account.

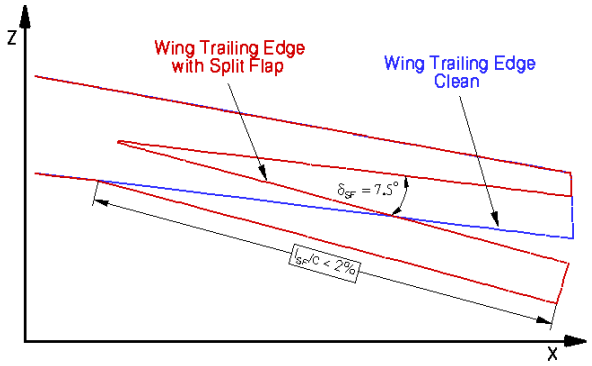

Fig. 2. Mini-TED geometry

According to wind-tunnel experiments and flight tests, the split-flaps with a relative length of less than 2% local chord were applied to the inboard and midboard parts of the wing (Fig. 3). The outboard portion of the wing remained unchanged.

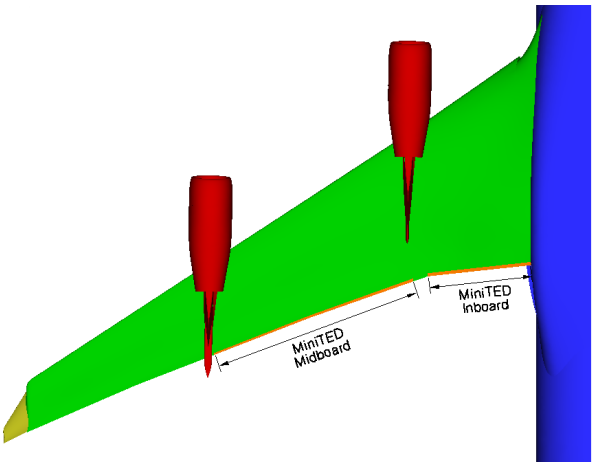

Fig. 3. AWIATOR aircraft with mini-TEDs deflected

4 Grid Generation and Computation

Both configurations of the AWIATOR aircraft were numerically simulated at wind-tunnel and free-flight conditions. Thus, the computations were performed at the cruise-flight Mach number M = 0.82 and at Reynolds numbers based on the aerodynamic mean chord of Re = 4.3 x 10^6 and Re = 45 x 10^6, respectively. For these four combinations of configuration and Reynolds number, a set of three cruise-flight lift coefficients $c_L \in [0.40, 0.50, 0.60]$ were considered.

For the numerical simulation of both aircraft configurations at both conditions a total of four hybrid grids were generated treating the aircraft as a half model with a symmetry plane. The grids were generated such that the surface grids of both configurations were nearly identical except for the wing trailing-edge region. Due to the large difference in the Reynolds number between wind-tunnel and free-flight condition, its impact on the boundary-layer development could not be neglected. For a good resolution of the viscous wing boundary-layer at both Reynolds numbers, the generation of 22 prismatic grid-layers was pre-adapted to the estimated height of the wing boundary-layer. The rest of the flow domain was filled with tetrahedra. The initial hybrid grids consisted of 5.8 x 10^6 grid nodes for the baseline aircraft configuration and of 10.1 x 10^6 grid nodes for the mini-TED aircraft configuration, respectively.

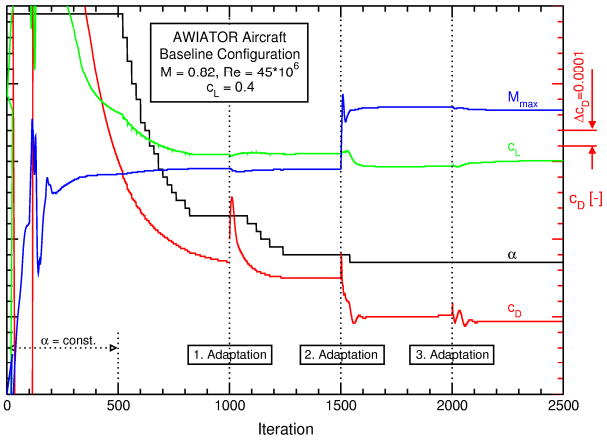

Fig. 4. Typical convergence history of a DLR-TAU RANS simulation

The TAU computations were performed using the central discretisation scheme, the multigrid-scheme 4W and the Spalart-Allmaras one-equation turbulence model with Edwards modifications [12]. The computations were conducted until the convergence to an overall steady-state solution was reached. Each computation was carried on, following a certain scheme containing several computation sequences and grid adaptations, until the aerodynamic coefficients were constant or the changes in the drag coefficient were smaller than one drag count (Δc_D = 0.0001) according to the accuracy of wind-tunnel data used for comparisons. This overall convergence also

included all grid adaptations performed. Fig. 4 shows a typical convergence history.

5 Results

The results of this numerical investigation will be presented in three sections. Firstly, the aerodynamic effect of mini-TEDs on the AWIATOR aircraft configuration is discussed for wind-tunnel conditions and the numerical results are compared with experimental data. Secondly, the influence of the Reynolds number on the mini-TED effect is analysed. And thirdly, a comparison of numerically predicted wing-surface pressure-distributions and measured flight-test data will be discussed for the baseline configuration.

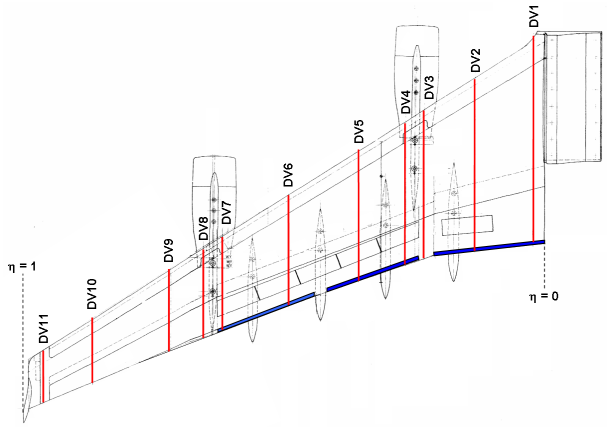

Fig. 5. Positions of pressure stations on the wing

In the following discussion besides lift curves and drag polars also wing-surface pressure-distributions in several sections will be shown. The positions of the pressure stations on the wing surface are shown in Fig. 5.

5.1 Mini-TED Effect at Wind-Tunnel Conditions

In general, the influence of mini-TEDs on the transonic airfoil flow is known. Previous investigations have shown that the mini-TED effect at transonic speeds is similar to that at low speeds [7]: the pressure distributions of the upper and lower airfoil sides are spreading at the trailing edge. The rear loading of the airfoil is increased considerably while the entire airfoil circulation is raised additionally. This leads to an increase in lift and drag as well as to a decrease in pitching moment at constant angle of attack. However, at constant lift coefficient the pressure distribution may be changed favourably so that drag is reduced. This effect occurs particularly at higher lift coefficients.

The aerodynamic effect of mini-TEDs on the complex three-dimensional AWIATOR aircraft configuration at cruise speed basically corresponds to the findings gained for two-dimensional airfoils. The influence on lift and drag can be seen in both the numerical results and the experimental data.

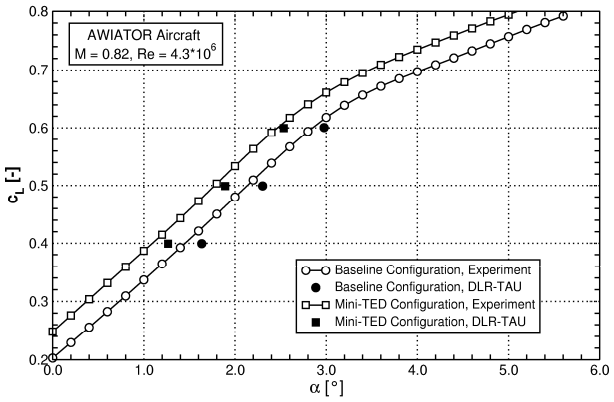

Fig. 6. Experimental and numerical lift curves at M = 0.82 and Re = 4.3 x 10^6

The comparison of numerical and experimental results is done using ONERA-S1MA wind-tunnel test data also produced within the AWIATOR project. Fig. 6 therefore shows the experimental lift curves and the numerical results for the baseline and the mini-TED configuration at wind-tunnel conditions with a Reynolds number of Re = 4.3 x 10^6. Both the experimental and the numerical data show a considerable lift increase due to the application of split-flaps. The results are qualitatively in good agreement. The numerical simulation reaches lower lift coefficients at constant angle of attack than measured in the experiment. Furthermore, the slopes of numerical and experimental lift curves ($dc_A/d\alpha$) are different for both configurations; the slopes of the numerical curves are slightly higher than those of the measured curves. Both findings are probably caused by geometric differences in the aircraft configurations between CFD and wind-tunnel model. In the numerical simulation both

tail-planes and the flap-track fairings were not considered whereas the vertical tail-plane and the fairings were present in the wind-tunnel model. The absence of flap-track fairings in particular leads to less lift at constant angle of attack since the fairings' geometry induces a lift enhancing effect on the flow, such as from a positively deflected flap. However, despite this general small lift-offset, the lift increase due to the mini-TEDs was numerically predicted also in good quantitative agreement.

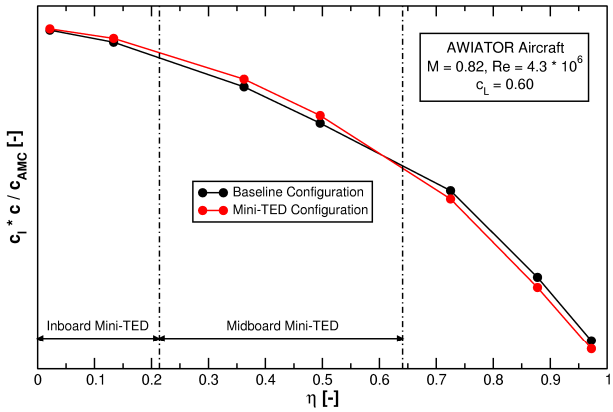

Fig. 7. Numerical wing-load distributions at M = 0.82, Re = 4.3 x 10^6 and c_L = 0.60

The application of mini-TEDs to the three-dimensional AWIATOR aircraft shows an influence reaching beyond the findings gained from two-dimensional studies. Since the mini-TEDs were not applied to the entire wing trailing-edge, the load distribution of the wing was changed such that the loading was transferred towards the wing root. Fig. 7 shows the spanwise wing-load distribution for the baseline and mini-TED configurations at wind-tunnel conditions and a lift coefficient of $c_L = 0.60$. The loading is increased in the inboard and midboard regions where the split-flaps are present on the wing. In regions without mini-TEDs, the loading is reduced compared to the baseline configuration since the angle of attack was decreased in order to keep the overall lift constant. This leads to a reduction of the wing-root bending-moment compared to the baseline configuration when using mini-TEDs.

Like the lift curves, the drag polars also exhibit a good qualitative agreement between numerical prediction and wind-tunnel measurements (Fig. 8). Similarly to the lift characteristics, here a small offset is also visible between the numerical and experimental data. Due to the absence of vertical tail-plane and flap-track fairings the numerical results exhibit less viscous drag than in the experiment. Since the viscous drag depends only little on the lift, Δc_D is nearly constant. The drag difference is seen to be on the order of the viscous drag of a vertical tail-plane and flap-track fairings.

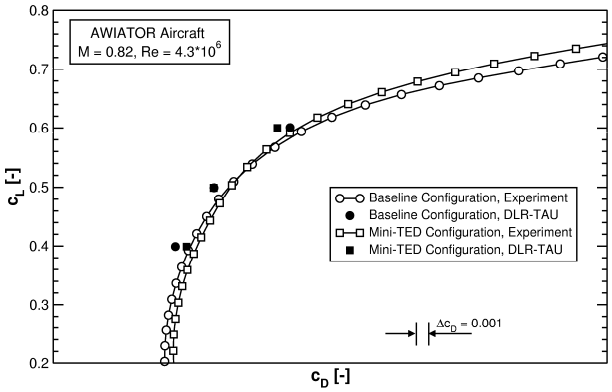

Fig. 8. Experimental and numerical drag polars at M = 0.82 and Re = 4.3 x 10^6

Concerning the mini-TED effect, the experimental drag polars exhibit higher drag coefficients for the mini-TED aircraft configuration than for the baseline configuration at lift coefficients $c_L \leq 0.52$. Around $c_L = 0.52$ the drag of both configurations is equal, whereas at lift coefficients $c_L \geq 0.52$ the mini-TED configuration achieves drag reductions. The numerical data exhibits approximately the same characteristics, but mini-TED and baseline configuration have the same drag coefficients at $c_L \approx 0.50$.

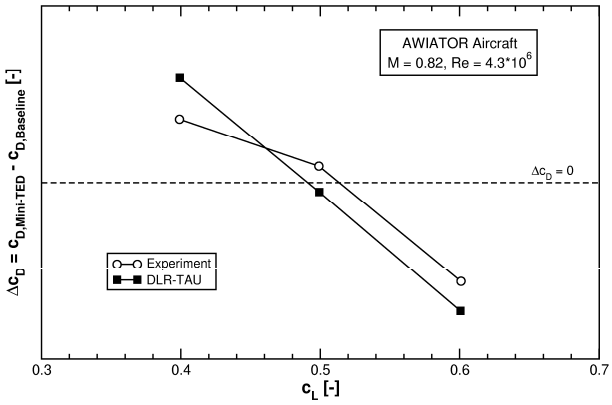

Fig. 9. Drag-difference curves for experimental and numerical results at M = 0.82 and Re = 4.3 x 10^6

The drag differences between the configurations calculated from the numerical and experimental data are shown in Fig. 9. The numerical data predicts a linear dependence between Δc_D and c_L being well reproduced by the experimental data at moderate and high lift coefficients with a small constant offset. However, at low lift the wind-tunnel experiment shows a smaller drag difference than in the numerical simulation. The reason for that is unclear.

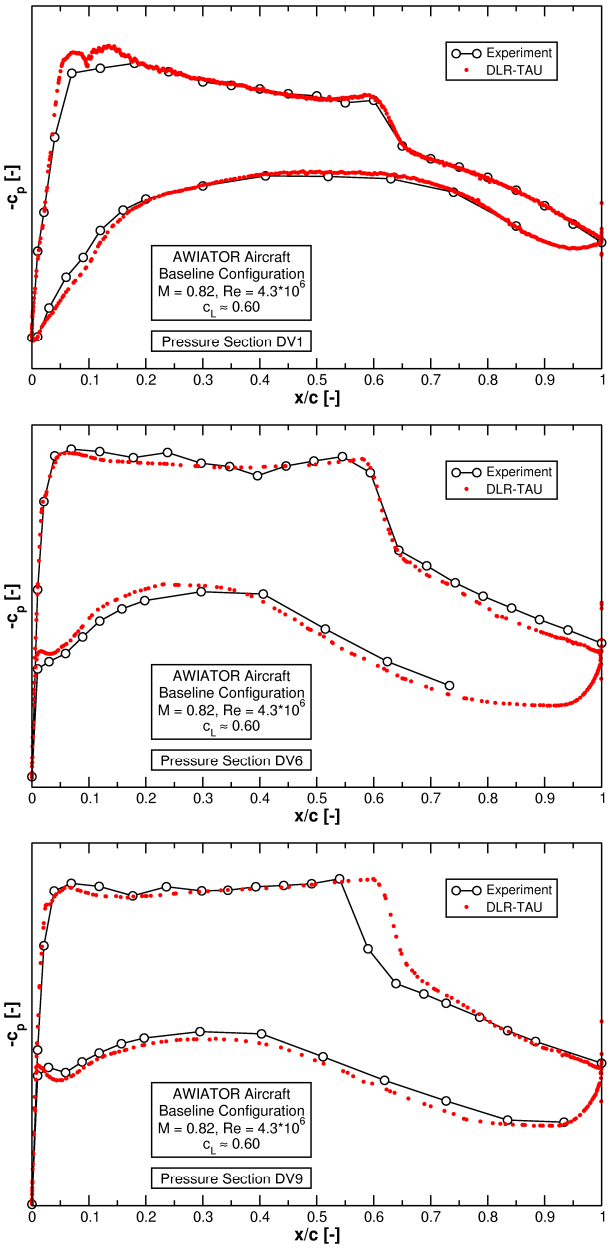

Fig. 10. Wing-surface pressure-distributions in sections DV1, DV6 and DV9 for the baseline configuration at M = 0.82, Re = 4.3 x 10^6 and c_L = 0.60

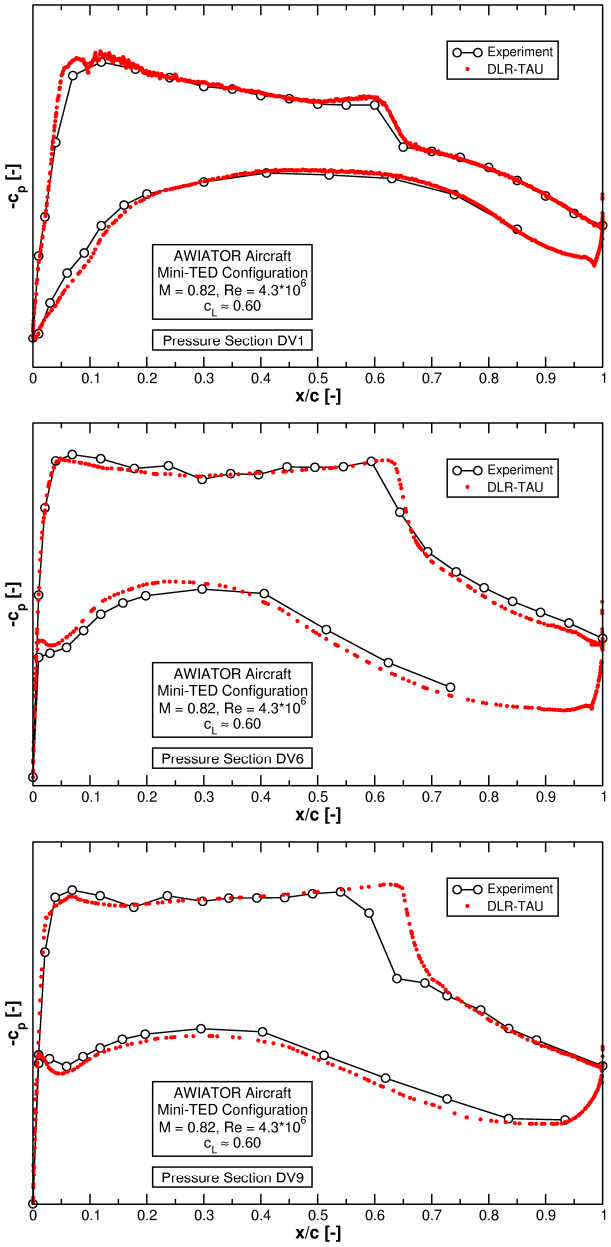

Fig. 11. Wing-surface pressure-distributions in sections DV1, DV6 and DV9 for the mini-TED configuration at M = 0.82, Re = 4.3 x 10^6 and c_L = 0.60

The good qualitative agreement of numerical and experimental results in terms of lift and drag is seen to originate from the correct prediction of the wing flow by the DLR-TAU code. To illustrate this, typical comparisons of the wing-surface pressure-distributions are given in Fig. 10 for the baseline configuration and in Fig. 11 for the mini-TED configuration for a lift coefficient of c_L = 0.60.

For the baseline configuration, the numerical and experimental pressure distributions in the inboard section DV1 show a

very good agreement. Shock position and trailing-edge pressure are predicted precisely by the DLR-TAU simulations, with only minor deviations appearing in the region of the suction peak. In the midboard section DV6 the agreement is also good; here suction-peak height, supersonic plateau and shock position are predicted correctly. However, deviations can be seen in the pressures of the lower side and the trailing-edge region on the upper side. Both maybe caused by the existence of flap-track fairings on the wind-tunnel model (see Fig. 5), leading to accelerated flow between these fairings on the lower side and at the trailing edge in the wind-tunnel experiment. Accordingly, in the outboard section DV9, where no flap-track fairings are present on the AWIATOR aircraft wing, the lower-side and trailing-edge pressures match properly again. The overall agreement is satisfactory although the shock position is predicted too far downstream, due to a twist of the model wing during the experiment.

The comparisons of numerical and experimental pressure distributions show similar good agreement for the mini-TED configuration. The pressure distributions in section DV1 also match well. The enhanced pressure difference at the trailing edge induced by the deflected mini-TEDs is reproduced precisely by the numerical simulation. In section DV6 the agreement is also good; here suction-peak height, height and length of the supersonic flow-field and thus shock position match very well. Only the fairing influence again leads to an increased trailing-edge pressure in the CFD results. However, the magnitude of the fairing induced Δc_p between experimental and numerical data is here the same as found for the baseline configuration. Since no mini-TEDs were present on the outboard part of the wing, the pressure distribution in section DV9 does not show the mini-TED effect. The pressure distribution here corresponds to the c_p-distributions of the baseline configuration. Due to the absence of flap-track fairings in this part of the wing in both wind-tunnel experiment and numerical simulation, the trailing-edge pressure is reproduced exactly. However, as seen for the baseline configuration, the overall agreement is here slightly worse than in the inboard and midboard sections due to the model deformation in the wind-tunnel experiment.

5.2 Reynolds-Number Influence on Mini-TED Effect

Besides the numerical simulation of the AWIATOR aircraft configurations at conditions of the wind-tunnel experiment, the simulations were also conducted at free-flight conditions. A comparison of low- and high-Reynolds-number results makes it possible to estimate the Reynolds-number influence on the aerodynamic effect of mini-TEDs. Since no high-Reynolds-number wind-tunnel tests were conducted in the framework of AWIATOR, the analysis of the Reynolds-number influence was only feasible by these RANS simulations.

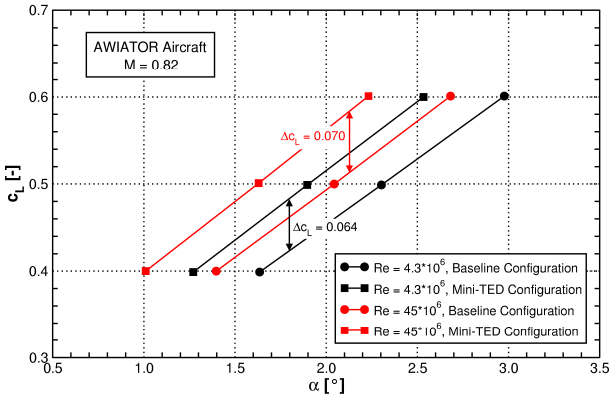

Fig. 12. Reynolds-number influence on lift curves

Fig. 12 shows the lift curves of baseline and mini-TED configurations at Re = 4.3 x 10^6 and Re = 45 x 10^6. As expected, the curves of both configurations at high Reynolds number are shifted to higher lift coefficients at constant angle of attack or to lower α at constant c_L, respectively. Additionally, the lift-enhancing effect of the mini-TEDs themselves increases. At Re = $4.3 \cdot 10^6$ the mini-TEDs provide a lift increase of $\Delta c_L \approx 0.064$, whereas for Re = $45 \cdot 10^6$ $\Delta c_L \approx 0.070$ is reached. This Δc_L-increase is a result of the thinner boundary layers at the high Reynolds number. For constant mini-TED size and deflection, the ratio of mini-TED height to boundary-layer thickness increases for increasing Reynolds number. The

same effect would be achieved by increasing mini-TED height at constant boundary-layer thickness or Reynolds number, respectively, causing the production of more lift by the mini-TED and thus raising its lift-enhancing effect.

Contrary to this clear Re-influence on the lift curves, the spanwise wing-load distribution is hardly changed due to the Reynolds number.

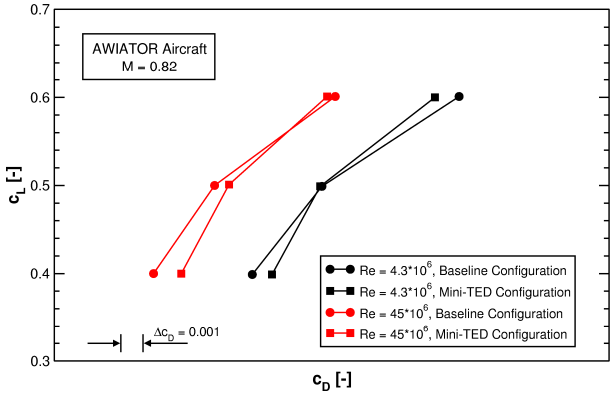

Fig. 13. Reynolds-number influence on drag polars

The drag polars for both configurations and Reynolds numbers are shown in Fig. 13. The polars at free-flight conditions exhibit less drag than at wind-tunnel conditions since viscous drag reduces with increasing Reynolds number. Beyond that, the different aircraft configurations exhibit slightly different drag characteristics at high Reynolds number. At low Reynolds number the mini-TED configuration reduces drag above a lift coefficient of $c_L \approx 0.50$. Thus, in the aircraft's aerodynamic design point at $c_L = 0.50$ the application of mini-TEDs begins to be profitable at $Re = 4.3 \times 10^6$. At $Re = 45 \times 10^6$ the lift coefficient of equal drag is shifted to higher values. A drag reduction here is not provided until $\Delta c_L \approx 0.57$ and a drag penalty has to be suffered at the design point. However, at $c_L = 0.60$ a drag reduction can still be obtained for the high Reynolds number, but less than at low Reynolds number. A detailed plot of the drag differences dependent on c_L and Re is given in Fig. 14. Similar to the increase of the lift-enhancing effect of mini-TEDs, the drag-difference curves are shifted to higher values for the free-flight Reynolds number. Drag reductions become smaller and even convert to drag increases for low and moderate lift coefficients.

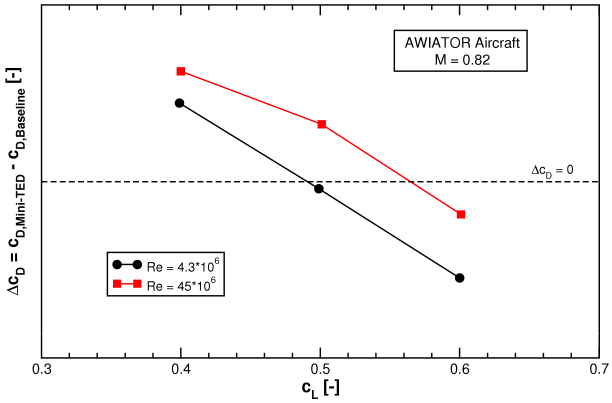

Fig. 14. Reynolds-number influence on drag difference

The change in the drag characteristics is explained by the wing-surface pressure-distributions. At low Reynolds number the mini-TEDs are working properly in the aircraft's design point and at higher lift coefficients along the entire wing span. The enhanced rear-loading due to the mini-TEDs here leads to a small reduction of shock strength when shocks are present in the wing flow of the baseline configuration (Fig. 15). When there are no shocks present, the enhanced rear-loading does no harm to the pressure distribution meaning drag is not increased. In the outboard region of the wing without mini-TEDs, a pure positive influence on the pressure distributions can be seen due to the reduced angle of attack for the aircraft in mini-TED configuration.

The situation is more complex at high Reynolds number: The mini-TEDs are still working properly in the inboard part of the wing; drag reductions are diminished but still appear. However, the midboard mini-TEDs are affecting the wing flow unfavourably. Drag reductions remain only at $c_L = 0.60$ whereas at low lift and in the aircraft's design point drag is increased since shocks are strengthened by the mini-TEDs (Fig. 15). Even in the outboard part of the wing where no mini-TEDs are present, the midboard mini-TEDs partly affect the flow unfavourably also leading to drag rises.

The analysis of the Re-influence shows that, for both the wind-tunnel and the free-flight condition, the mini-TED deflection of $\delta_{SF} = 7.5°$ applied to the AWIATOR aircraft is properly chosen in the inboard part of the wing. For the midboard part of the wing the pressure

distributions show that the mini-TED deflection is too high for both conditions at low and moderate lift. Only at a high lift coefficient of $c_L = 0.60$ are the mini-TEDs seen to be not too high since drag reductions can still be achieved. However, these drag reductions are smaller in free-flight than at wind-tunnel conditions.

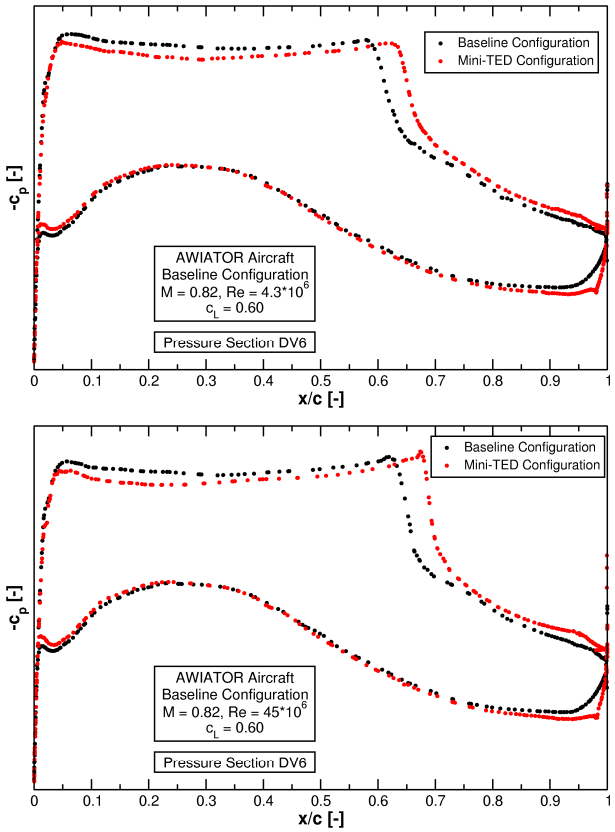

Fig. 15. Wing-surface pressure-distributions in section DV6 for both configurations at M = 0.82, $c_L = 0.60$ for Re = 4.3 x 10^6 and Re = 45 x 10^6

5.3 Comparison with Flight-Test Data

As shown in section 5.1, the TAU-Code proved its ability in the prediction of the mini-TED effect on the AWIATOR aircraft configuration and its capability to deal with the complex flow around a split-flap. After determining the Reynolds-number influence on the mini-TED effect, the consistent next step would be to prove the prediction capabilities also for free-flight conditions and to verify the predicted Reynolds-number influence. Since not all necessary flight tests have been conducted yet, this goal cannot be met at this time. However, in a first step, in-flight pressure distributions of the baseline aircraft configuration are already available.

The comparison of numerical and flight-test c_p-distributions in general shows a good agreement for all pressure-sections considered. As an example, Fig. 16 shows the pressure distribution at section DV6 for the baseline configuration at a lift coefficient of $c_L = 0.60$. Here, the numerical and the flight-test data match very well. Since the real aircraft wing is undergoing a twist during the flight, the agreement of the pressure distributions is slightly worse at stations on the outboard part of the wing. Particularly the shock position is very sensitive to the local angle of attack and is predicted too far downstream compared to its position on the twisted wing. However, when compensating the wing twist with a reduced α, a good overall agreement of the pressure distributions is reached also in the outboard region of the wing.

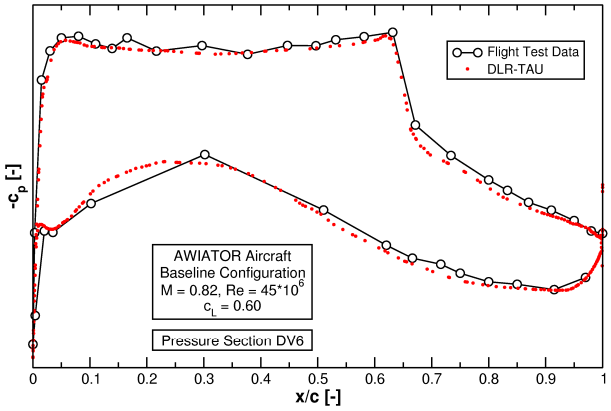

Fig. 16. Wing-Surface Pressure-Distributions in Section DV6 for the Baseline Configuration at M = 0.82, Re = 45 · 10^6 and $c_L = 0.60$

6 Conclusions

Within task T3.3 of the European research project AWIATOR a numerical investigation on the aerodynamic effect of mini-TEDs on an Airbus A340-300 was conducted at wind-tunnel and free-flight conditions for cruise-flight Mach number M = 0.82 and lift coefficients $c_L \in [0.4, 0.5, 0.6]$. Therefore the AWIATOR aircraft configuration with and without mini-TEDs applied to the wing trailing-edge was investigated. Both configurations were

simulated without tail-planes or flap-track fairings. The mini-TEDs were realised by split-flaps with a length of less than 2% local wing chord and a deflection of $\delta_{SF} = 7.5°$. The mini-TEDs were applied to the inboard and midboard part of the wing whereas the outboard part remained unchanged. The numerical simulation was conducted using the DLR-TAU code. Grids were generated using the commercial grid generator CENTAUR™.

The numerical results achieve a good agreement with data provided by ONERA-S1MA wind-tunnel experiments in terms of lift and drag. The DLR-TAU code proves to be capable of predicting the mini-TED effect on the aircraft aerodynamics properly. With mini-TEDs applied, lift is increased and redistributed towards the wing root leading to drag reductions at moderate and high lift coefficients. Comparisons of wing-surface pressure-distributions prove these lift and drag characteristics in detail and show a good agreement with the experimental data for all wing sections.

The Reynolds-number influence on the mini-TED effect was evaluated. At free-flight conditions, the mini-TED effect is seen to increase compared to wind-tunnel conditions. Here, the lift-enhancing effect of the mini-TEDs increases but the drag differences compared to the baseline configuration are affected unfavourably. The minimum lift coefficient of profitable mini-TED use is shifted to higher lift. Remaining drag reductions at high lift coefficients diminish and in the aircraft's design point at $c_L = 0.50$ a drag penalty has to be suffered. At free-flight conditions, the deflection angle of $\delta_{SF} = 7.5°$ is seen to be properly chosen for in the inboard mini-TED but to be too high for the midboard mini-TED. These findings indicate that mini-TEDs cannot achieve optimum performance on a wing not designed for their application and should therefore be included in the aerodynamic design of the wing.

Additional comparisons of numerical and flight-test pressure distributions of the baseline configuration show a good overall agreement and moreover proves the capability of the DLR-TAU code to predict the high-Reynolds-number flow around complex aircraft configurations.

References

[1] Hansen H. Application of mini trailing edge devices in the AWIATOR project. *5th ONERA-DLR Aerospace Symposium*, Toulouse, France, 2003.

[2] Hansen, H. Application of adaptive trailing edge elements within the AWIATOR project. *CEAS/KATnet Conference on Key Aerodynamic Technologies*, Bremen, Germany, 2005.

[3] Jeffrey D., Zhang X., Hurst D.W. Aerodynamics of Gurney flaps on a single-element high-lift wing. *Journal of Aircraft*, Vol. 37, No. 2, pp. 295-301, 2000

[4] Ross J.C, Storms B.L., Carrannanto P.G. Lift-enhancing tabs on multielement airfoils. *Journal of Aircraft*, Vol. 32, No. 3, pp. 649-655, 1995

[5] Myose R., Papadakis M., Heron I. Gurney flap experiments on airfoils, wings, and reflection plane model. *Journal of Aircraft*, Vol. 35, No. 2, pp. 206-211, 1998

[6] Henne P.A., Gregg R.D. New airfoil design concept. *Journal of Aircraft*, Vol. 28, No. 5, pp. 300-311, 1991

[7] Richter K., Rosemann H. Experimental investigation of trailing-edge devices at transonic speeds. *The Aeronautical Journal*, Vol. 106, No. 1058, pp. 185-193, 2002

[8] Gerhold T., Friedrich O., Galle M. Calculation of complex three-dimensional configurations employing the DLR-TAU-code. *AIAA 35th Aerospace Sciences Meeting & Exhibit*, Reno, USA AIAA-97-0167, 1997.

[9] Schwamborn D., Gerhold T., Kessler R. The DLR-TAU code – an overview. *1st ONERA-DLR Aerospace Symposium*, Paris, France, 1999.

[10] Spalart P.R., Allmaras S.R. A one-equation turbulence model for aerodynamic flows. *AIAA 30th Aerospace Sciences Meeting & Exhibit*, Reno, USA AIAA-92-0439, 1992.

[11] http://www.centaursoft.com

[12] Edwards J.R., Chandra S. Comparison of eddy viscosity-transport turbulence models for three-dimensional, shock-separated flowfields, *AIAA Journal*, Vol. 34, No. 4, 1996

Acknowledgements

The research project (Technology Platform) AWIATOR is supported by the European Commission under the 5th Framework Programme.